The Geometry and Temporal Structure of a High Frequency Source: The Olyutorskii Earthquake of April 20, 2006

A. A. Gusev[a, b] and E. M. Guseva[b]

[a] *Institute of Volcanology and Seismology, Far East Division, Russian Academy of Sciences, Petropavlovsk-Kamchatskii, 683006 Russia*

[b] *Kamchatka Branch, Geophysical Service, Russian Academy of Sciences, Petropavlovsk-Kamchatskii, 683006 Russia*

Received May 10, 2008

Abstract—We have determined the parameters of the high frequency radiator for the $M_W = 7.6$, April 20, 2006 Olyutorskii earthquake using *P*-wave high frequency power signal (HFPS), as recorded at 57 distant stations. Our data processing was done, first, to correct the HFPSs by inverse filtering using the aftershock HFPS as an empirical power Green's function. In this way, we found the source HFPS for each station, separately for the frequency bands 0.7–1.7 and 1.5–2.5 Hz. These data were used to determine parameters of the radiator model as a segment with the rupture propagating to both sides of the hypocenter at constant velocity. The parameters are as follows: length 128 ± 52 km, the strike of the longer arm of the rupture $225° \pm 19°$ SW, the distance from the epicenter to the centroid 23 ± 9 km, and rupture velocity 2.5 ± 0.8 km/s. The rupture was bilateral with a moderate asymmetry. The rupture duration was 35.0 ± 1.6 s for the southwestern arm and about 23 s for the northeastern.

INTRODUCTION

This study is concerned with the general structure of the large ($M_W = 7.6$) Olyutorskii earthquake, which occurred on April 20, 2006 in Koryakia, Northeast Russia, which was previously considered to be a low seismicity area. The high-frequency radiator that operated at the earthquake source was reconstructed using the approach that was previously put forward and developed by A.A. Gusev and V.M. Pavlov [1–8]. We use high-frequency power signals (HFPS) of teleseismic *P* waves stations, which are estimated as the squared amplitude after bandpass filtering. Distortions in a HFPS as the signal is propagating along a scattering path were corrected by inverse filtering of the mainshock HFPS at several stations using the HFPS of an aftershock as an empirical Green's function. Similar approaches to the reconstruction of a high frequency radiator, although not quite identical with the one we are using here, were also suggested in a number of other publications [9–12]; these studies used theoretical Green's functions or empirical Green's functions determined as small-earthquake HFPSs averaged over the region of interest, or else scattering was disregarded altogether. The result of inverse filtering consists in estimated HFPSs radiated by the rupture. These signals are parameterized and, at the last step, the parameters are used to infer important spatio–temporal source parameters.

The earthquake rupture was bilateral and very close to being symmetrical; this fact has greatly complicated the inversion. For this reason we have not succeeded in describing the rupture in a model-independent way, as was proposed in [1, 2, 4–7]. Instead we used a simple parametric model consisting of a straight segment with constant luminosity which is ruptured bilaterally at constant velocity. We parameterized the source HFPS to determine the model parameters from temporal power moments of degrees 1 and 2 with the addition of the total HFPS duration. This modification of the technique yielded acceptable results.

THE THEORETICAL BASIS OF THE TECHNIUQE

We begin by discussing the technique for reconstructing the source HFPS. As this was recently described in detail [8], we shall restrict ourselves to a brief summary. Consider the high frequency power signal (HFPS) for for a certain source — station pair, which is the smoothed function $M(t)$ of the instantaneous mean square amplitude, for a definite frequency band Δf with a sufficiently high central frequency *f*. For example, the frequencies 0.5–2.0 Hz can be considered to be high for teleseismic *P*-waves excited by $M > 7$ earthquakes. The signal $M(t)$ is distorted by scattering and multipathing. It is desired to estimate the HFPS $P(t)$ that would have been observed in the ideal case of a nonscattering homogeneous earth. In actual practice $P(t)$ is understood to be a *P*-wave signal that was directly radiated by an earthquake source, or the "source HFPS." We make two assumptions: (1) the pulse response of the earth for power, or the power Green's function *A* is

slowly changing within the radiating fault plane; (2) the smoothed squared aftershock record $A(t)$ can be regarded as an estimate for $A_0(t)$ or as an empirical power Green's function (this includes P, pP, sP, and the P-coda in the first place). We further assume that the observed filtered seismograms of the main shock and the aftershock (before being squared) can be treated as incoherent signals (that is, we assume them to have approximately random phases and to be pairwise uncorrelated). It can then be assumed that, approximately, we have $M(t) = A(\cdot)*P(\cdot)$, where * denotes convolution. In that case $P(t)$ can be estimated by applying to $M(t)$ the inverse filter based on $A(t)$. Write down the discrete convolution in matrix form as $\mathbf{AP} = \mathbf{M}$, where $\mathbf{A}$ is the Toeplitz matrix that represents $A(t)$. We obtain linear equations for the components of the vector $\mathbf{P}$. The equations are certainly overdetermined, since $M(t)$ and $A(t)$ involve the coda, while $P(t)$ does not contain it. An overdetermined set of equations can be solved by least squares (LS). We also imposed an extra requirement, namely, that $P(t)$ should be nonnegative, as being a power signal. The Lawson–Hanson NNLS algorithm was used. The estimates of the $P(t)$ can subsequently be used to extract information on the source; to do this, these functions should first be parameterized.

With the above approach, we used the $P(t)$ to find their temporal power moments. We used the moments of degree 1 (temporal centroids) $e_k^{(1)}$, the temporal central moments of degree 2 $e_k^{(2)}$, as well as total duration T_{fk}, the subscript k referring to the particular station. The time origin is the onset time in the procedure of determining moments of degree 1 and total duration. We make it clear that the value of $((e_k^{(2)})^{0.5}$ is the "temporal radius of inertia" of the power pulse, or its rms duration. It can be seen from the equations in [2, 5] that the parameters $e_k^{(1)}$, $e_k^{(2)}$ can be used to find normalized spatio–temporal power moments of the radiator: the vector of the first moments (N_t, N_x) and the second central moments $\{N_{tt}, N_{tx}, N_{xx}\}$, where $\mathbf{x} = (x, y, z)$ and the axes are as usual oriented as follows: x northward, y eastward, and z downwards.

The estimates that are derived by this procedure have the following meanings. The vector N_x gives the position of the radiator's centroid relative to the hypocenter, and N_t is the mean time delay of the radiation relative to the origin time (the temporal centroid). The tensor N_{xx} gives the spatial extent of the radiator, the scalar N_{tt} is related to the temporal extent of the radiating process, while the vector N_{tx} characterizes the spatial directivity of the process. When data are available on the high frequency radiation from a shallow earthquake with magnitude greater than 7, whose vertical source extent is small compared with the horizontal, it is impossible to determine the parameters related to the vertical coordinate z with satisfactory accuracy, as only the moments in the horizontal

plane and the temporal moments can be estimated. Ultimately only the three first and the six second moments are retained. The remaining moments can be set equal to zero in the case of a source whose main extent is horizontal.

The hypothesis is realistic for crustal earthquakes with $M > 7$–7.2 and for subduction earthquakes with $M > 7.6$–7.7. The April 20, 2006 Olyutorskii earthquake is a crustal $M = 7.6$ event, hence the approach we have outlined is justified. The subsequent discussion will be concerned with the vector of the 1st moments $\mathbf{M1}$ or $\{M1_t, M1_x, M1_y\}$ and with the 6-vector of the 2nd moments $\mathbf{M2}$ or $\{M_{tt}, M_{xt}, M_{yt}, M_{xx}, M_{xy}, M_{yy}\}$.

In addition to the moments, we also determined the position of the rupture termination point in space–time (relative to the epicenter and the origin time). This position is described by the vector $\mathbf{F}$ or $\{F_t, F_x, F_y\}$. The vector was determined using total durations T_{fk} of the reconstructed source HFPSs. The equation that relates $\{F_t, F_x, F_y\}$ and T_{fk} is the same as the equation connecting $\{M1_t, M1_x, M1_y\}$ and the $e_k^{(1)}$.

THE DATA AND THE DATA PROCESSING

Our data set consisted of 57 pairs of P-wave records at BHZ channels of worldwide digital seismic stations retrieved through the IRIS DMS Data Center. Each pair was a record of the main shock (23:25:05 UT, April 20, 2006, epicenter at 61.0° N, 167.1° E, depth 10–20 km, $M_w(\text{HRV}) = 7.6$) and a record of the aftershock (04:32:45 UT, April 21, 2006, epicenter at 60.6° N, 165.8° E, depth 18 km, $M_w(\text{HRV}) = 6.1$). The station's azimuth and distance can be seen in Fig. 1. The first step was to do a bandpass filtering for each station in two frequency bands: (1) 0.7–1.7 and (2) 1.5–2.5 Hz, to estimate the signals $M_k(t)$ and $A_k(t)$, to reconstruct the signals $P_k(t)$, and to calculate the parameters $e_k^{(1)}$, $e_k^{(2)}$, and T_{fk}. Ordinary least squares was then applied to the sets of linear equations which relate, for each frequency band, the unknown components of $\mathbf{M1}$, $\mathbf{M2}$, and $\mathbf{F}$ to elements of the data sets $e_k^{(1)}$, $e_k^{(2)}$, and T_{fk} using the weights to be discussed later. The solutions for $\mathbf{M1}$ and $\mathbf{F}$ were acceptable, while the estimation of $\mathbf{M2}$ faced some difficulties in that formal estimates do emerge, but the resulting combination M_{xx}, M_{xy}, M_{yy} is unacceptable from physical considerations. This issue is discussed in more detail later. It thus appears that, in our case, there was merely a theoretical possibility of reconstructing the complete set of second moments, and it has not been possible to derive a nonparametric description of the source in terms of the set of moments of degrees 1 and 2. In this situation we had to restrict ourselves to characterizing the source rupture in terms of a parametric model. To do this, we used the position of rupture termi-
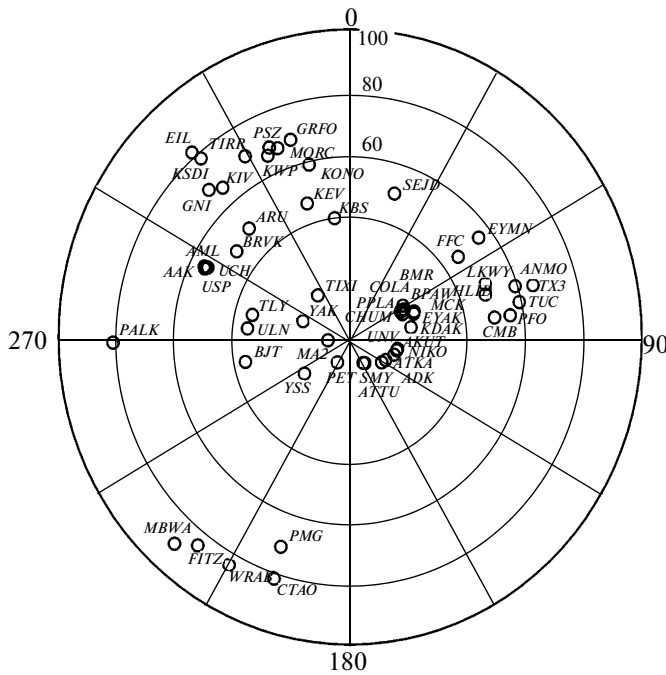
Fig. 1. The distribution of stations over azimuth and epicentral distance.

nation point and the time of rupture termination (relative to t_0) which is described by the spatio-temporal vector **F**. Combining the well-constrained moments and the parameters of the rupture termination point, one can manage to find the parameters of the source model. The model is assumed here to be a (horizontal) straight segment with constant luminosity; the rupture front ("the "luminous point") propagates in both directions at identical and constant velocities from some point of the segment. The model involves four parameters: (1) segment length L, (2) segment azimuth α (of the two azimuth variants we selected that which gives the sense of rupture propagation for the longer arm of a bilateral rupture), (3) distance d between the epicenter (the point of rupture initiation) and the radiator's centroid (the middle of the source segment), and (4) rupture velocity v_r. This model will be referred to as the "linear segment model" in what follows.

The data processing procedure is illustrated for the YAK station in Figs. 2−4. The top plot in Fig. 2 is an ordinary seismic signal, the Z displacement for the main shock. Under this are filtered records for both of the frequency bands used here. Before filtering we transformed the BHZ records to acceleration and corrected for attenuation along the ray; the result was a signal with an approximately flat spectrum that is optimal in the sense of information content. Figure 3 shows the squared amplitude of the mainshock and

aftershock (estimates of HFPSs) after smoothing with a 1-s window and decimation at the same step (binning).

Figure 4 illustrates inverse filtering (deconvolution). Figures 4a and 4b show (in the middle plots) how $M(t)$ is fitted by a convolution of $A(t)$ with the function $P(t)$ estimated by the inversion. The estimate itself of the source rupture signal $P(t)$ is shown in the bottom plot. We calculated $e_k^{(1)}$ and $e_k^{(2)}$ for each $P(t)$ in each of the two bands. The value of T_{fk} was found by joint examination of $P(t)$ on the two channels simultaneously, which is illustrated in Fig. 4c. The quality of reconstruction for the function $P(t)$ varied considerably from channel to channel and from station to station, so that each estimate of the function was ascribed a weight to be used subsequently in least squares calculations based on the corresponding values of $e_k^{(1)}$, $e_k^{(2)}$, and T_{fk}. We used four weight options: 1.0 (quite acceptable), 0.2 (not quite reliable), 0.04 (barely acceptable), and 0 (unacceptable).

For band 1 we obtained 57 pairs of estimates for $e_k^{(1)}$, and $e_k^{(2)}$, and 43 pairs for band 2; the estimate of T_{fk} was obtained at 55 stations. The estimates are summarized in Table 1.

Figure 5 illustrates the general character of the $P(t)$. One notes an azimuthal asymmetry of $P(t)$ durations, the shortest records being in the southwest and the longest in the northeast sector. This difference arises from the Doppler effect due to the prevailing southwestward rupture propagation.

The next step was to solve the equations for the components of **M1**, **M2**, and **F**. The quality of LS fits is apparent from Fig. 6. The residuals are not small. That means that the reconstruction of $P(t)$ involves considerable distortions, probably due to the large fluctuation noise that the original HFPSs contain. The noise arises because of a very limited signal band (1 Hz) and a limited rupture duration (a few tens of seconds). This results in large error margins for the components of **M1**, **M2**, and **F**, while the estimates themselves are insufficiently stable. The instability causes the greatest unpleasantness when estimating the vector **M2** where it is known beforehand that its three components $\{M_{xx}, M_{xy}, M_{yy}\}$ must make up a positive definite matrix (the source "inertia tensor"), while the matrices composed of the actual estimates are not positive definite. Restricting ourselves for the moment to an analysis of the estimates of **M1** and **F** (Table 2), we have been able to determine:

(1) the prevailing rupture direction: three mutually consistent, independent estimates indicate a southwestward direction, their mean is $\alpha = 219° \pm 14°$. However, considering that the vectors **M1** themselves are relatively short compared with **F**, we shall estimate the rupture
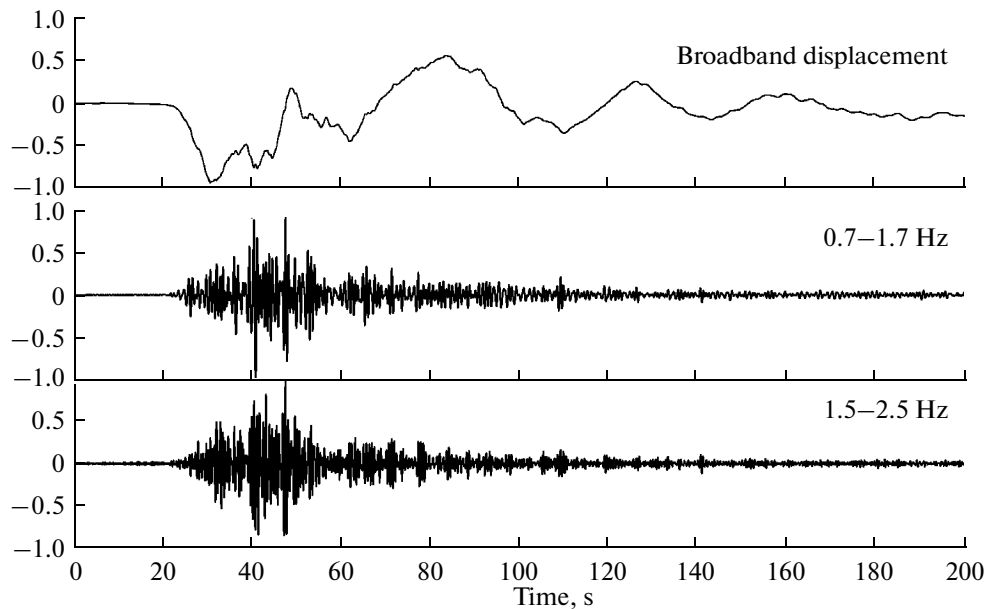
Fig. 2. An example record of high frequency *P*-waves (the Yakutsk (YAK) broadband station). Top: broadband displacement on the *Z* record (BHZ) for the main shock. Middle and bottom: same signal after preprocessing.
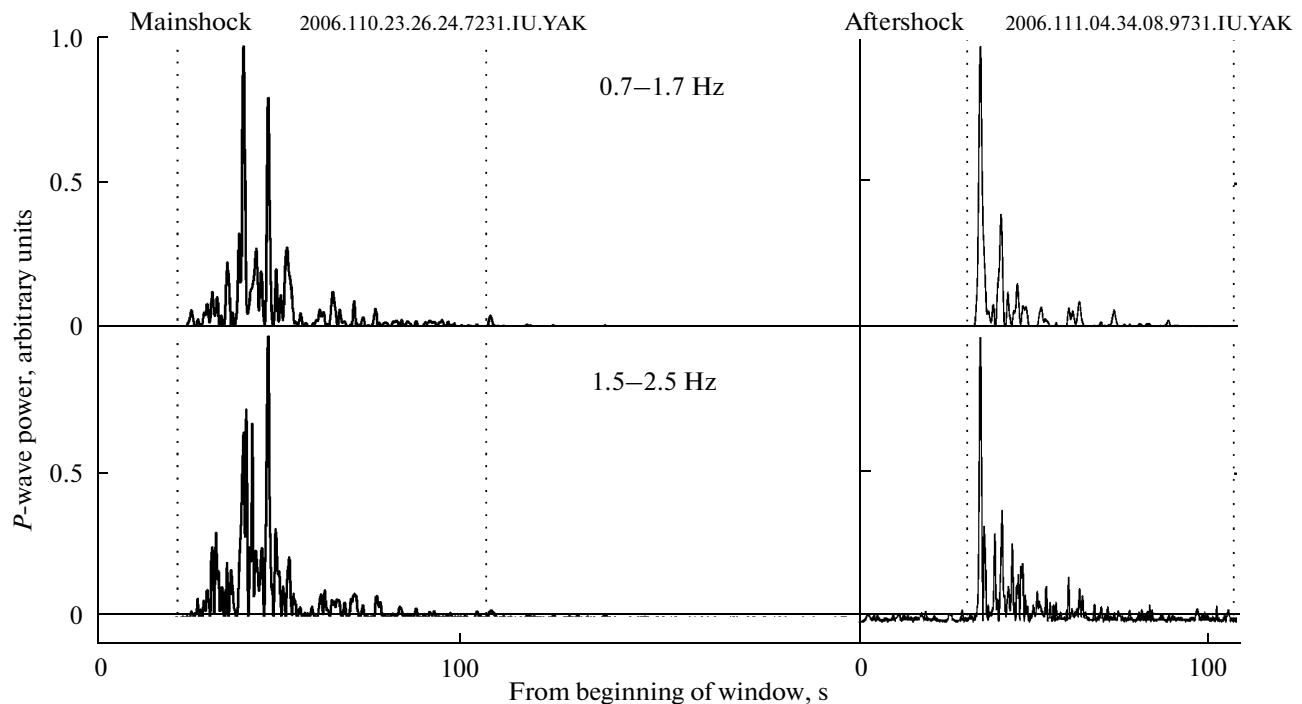

Fig. 3. Squared amplitude after being smoothed by a 1-s window (high frequency power signal, HFPS) for the main shock and the 04 h, April 21, 2006 aftershock at the YAK station. Vertical dotted lines indicate the time windows chosen interactively for selecting the data segment to be processed.

strike by adopting the estimate based on **F**: $\alpha = 225° \pm 19°$; (2) the distance from the epicenter to the radiator's centroid (the two estimates when averaged give $d = 23 \pm 9$ toward southwest; (3) the rupture duration ($F_t = 35.0 \pm 1.6$ s); (4) the position of rup-

ture termination point relative to the epicenter ($F_L = 87 \pm 28$ km to southwest); (5) rupture velocity $v_r = 2.50 \pm 0.8$ km/s.

We emphasize that all these parameters are assigned the uncertainty estimates that are either obtained in a
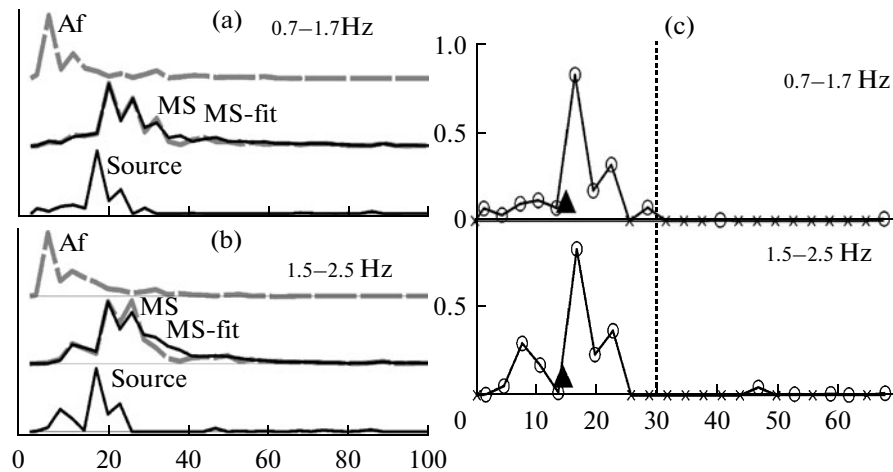
Fig. 4. An example reconstruction of the source HFPS for YAK: (a) mainshock HFPS (MS for main shock) and the aftershock HFPS (Af for aftershock) after being smoothed by a 3-s window and decimated (gray lines); "Source" denotes the reconstructed source HFPS for the ray toward YAK; MS-fit denotes the fit to the MS signal (grey) by the NNLS algorithm for the band 0.7−1.7 Hz, (b) same for the band 1.5−2.5 Hz. (c) selecting the estimate of T_f based on the source HFPS in two bands (vertical dashed line), positive (circles) and zero (crosses) data values for the reconstructed source HFPS are marked; the temporal centroid $e(1)$ is marked by a triangle.

straightforward manner from the LS results or by the method of error propagation.

Next the parameters of the linear segment model were to be determined. It is easily seen that in the framework of this model the length of the longer rupture arm (equal to F_L), the total rupture length L, and the epicenter–midsegment distance d are related by the simple relation $L = 2(F_L - d)$. Inserting the estimates of F_L and d given above, we get $L = 128 \pm 56$ km.

We are now in a position to try to extract additional information from the estimates of $e_k^{(2)}$, whose forward inversion has been a failure. To do this, we first fix the values of the poorly constrained components M_{xx}, M_{xy}, and M_{yy} of the vector **M2** based on our estimates of rupture length ($L = 128$ km) and rupture orientation (strike) (39NE−219SW). A few words of explanation are in order. The directions of the eigenvectors of the matrix M_{ij} (where $i, j = x, y$) are totally unrelated to the direction of the vector $\{M_{xt}, M_{yt}\}$ in the framework of the source second moments formalism, so that the estimate of the last vector is still meaningful in spite of the fact that M_{ij} has been fixed.

The estimate for the component M_{tt} depends on the choice of L. However, although real, this dependence is actually rather weak. It follows that the above approach is quite meaningful. The rupture fault width was set equal to 25 km; the choice of this poorly known parameter in a wide reasonable range (15−40 km) does not nearly affect the result. The resulting estimates of M_{tt} and other components of **M2** (derived by LS with constraints) are summarized in Table 3.

Since the rupture length L involves a large uncertainty, an erroneous choice of its value might, generally speaking, distort the estimates of M_{tt}, M_{xt}, and M_{yt}. We have tested whether this danger is real by repeating the calculation for two additional options for L, 72 and 184 km (variations within $\pm 1\sigma$ about the main estimate 128 km). It turned out that the estimates of M_{tt}, M_{xt}, and M_{yt} are not very sensitive to the choice of a fixed value of L; the variation due to the deviations of L do not exceed 5%. A crude estimate of the total error (the LS error and an additional error due to the uncertainty in L) is approximately 10% for M_{tt}, while the direction of the mixed-moments vector M_{xt}, M_{yt} can be found to within 40−50°, not better.

We now turn to a discussion of the meaning of these estimates. The direction of the vector M_{xt}, M_{yt} in the linear segment model ought to be identical with that of the vectors $\{M1_x, M1_y\}$ and $\{F_x, F_y\}$, which is close to 219°. The actual estimate of the direction of M_{xt}, M_{yt} is little different, to within 10°. This is an important independent confirmation that the above reconstruction of the rupture parameters from the 1st moments is correct. The temporal moment of degree 2 M_{tt} provides a new estimate for the rupture duration, which is assumed to be a rectangular pulse; this is equal to $T^{(2)} = 3.45 M_{tt}^{0.5}$ ($3.45 = 12^{0.5}$ is the length of a segment whose rms length is unity). The estimate averaged over the frequency bands is $T^{(2)} = 28.5$ s. The uncertainty of that parameter is about ± 2 s.

The next stage of our discussion will be a joint interpretation of these results (Fig. 7).

The radiator's centroid. Combining the vector $\{M1_x, M1_y\}$ and the instrumental epicenter as reported by the

Table 1. Temporal parameters of power signals recorded at individual stations

Station code	$Az°$	$\Delta°$	T_f	$e_1^{(1)}$	$e_2^{(1)}$	RT_1	RT_2	$w(T_f)$	$w(1)$	$w(2)$
SFJD	017	49.9	42	15.3	18.2	11.8	11.1	0	0.04	0.04
EYMN	053	55.1	45	15.0	7.3	10.7	5.2	0.04	0.2	0.04
FFC	053	45.7	39	13.1	–	9.7	–	0.04	0.2	0
COLA	058	21.2	33	14.3	14.2	8.6	7.8	0.04	1	0.04
BPAW	061	20.0	30	14.4	13.6	8.9	7.5	0.2	0.2	1
MCK	061	21.0	30	15.2	14.3	10.2	8.1	0.04	0.04	0.2
CHUM	062	19.5	42	15.9	18.0	8.5	9.0	0.04	0.04	0.2
PPLA	065	19.7	36	14.4	14.3	6.5	8.8	0.2	1	1
BMR	067	23.7	33	9.8	17.5	7.3	8.8	0.04	1	1
LKWY	068	49.7	39	16.6	17.1	10.2	12.1	1	1	1
EYAK	068	23.3	27	10.3	8.1	6.8	7.0	0.04	0.2	0.04
HLID	072	48.6	36	11	–	11.5	–	0.2	0.2	0
ANMO	072	59.2	45	21.2	–	10.9	–	0.2	0.2	0
TX32	074	65.1	42	19.1	19.5	10.2	7.5	0.04	1	1
TUC	078	59.2	54	22.3	24.1	14.3	12.2	0.04	0.04	0.04
KDAK	079	21.2	33	9.5	9.6	9.6	6.0	0.04	0.2	0.2
CMB	081	50.0	54	19.6	20.5	12.3	12.3	0.2	0.04	0.04
PFO	081	55.4	42	18.4	19.7	10.4	7.8	0.2	1	1
AKUT	100	16.5	39	20	16.6	13.9	9.8	0.2	0.2	0.2
UNV	102	16.3	30	15.3	15.6	6.9	4.9	0.04	0.2	0.2
NIKO	107	15.7	30	8.1	–	9.3	–	0.04	0.04	0
ATKA	118	13.8	36	17.6	13.1	9.7	10.7	1	1	0.2
ADK	124	13.0	36	20.0	20.6	9.2	8.2	0.2	0.2	0.2
SMY	146	9.1	12	4.15	5.9	2.9	2.9	0.04	0.04	0.04
ATTU	149	8.7	36	21.3	19.2	9.4	9.5	0.04	0.2	0.2
CTAO	198	81.9	39	16.1	14.3	9.4	11.6	1	1	1
PMG	199	71.3	39	18.1	–	9.1	–	0.04	0.04	0
WRAB	209	84.1	33	10.7	6.5	8.8	6.9	0.04	0.2	0.04
PET	210	8.5	18	3.9	9.8	2.4	4.6	0.2	1	1
FITZ	218	84.8	36	12.8	9.5	7.7	7.1	0.04	0.2	0.04
MBWA	222	89.5	33	11.2	10.1	8.3	6.8	0.2	1	1
YSS	234	19.1	27	16.4	–	7.0	–	0.2	1	0
BJT	258	36.6	30	15.4	–	8.1	–	0.04	1	0
MA2	268	7.5	24	15.5	12.1	6.9	2.5	0.2	1	1
PALK	269	81.3	33	14.7	15.6	7.6	6.8	0.2	1	1
ULN	276	35.3	36	15.3	13.4	10.1	7.9	0.04	1	0.04
TLY	283	34.5	30	16.8	13.7	6.6	8.0	0.04	0.2	0.04
YAK	290	17.2	27	18.3	17.4	5.2	4.5	1	1	0.2
UCH	294	54.9	30	14.1	–	6.7	–	0.04	0.04	0
AAK	295	54.6	27	13.9	8.7	8.6	5.8	0.2	0.2	0.2
AML	295	55.4	24	12.1	–	7.6	–	0.04	0.2	0
USP	295	54.1	42	17.0	10.8	9.7	6.7	0.2	1	0.2
BRVK	306	48.3	33	14.1	11.9	7.3	4.1	0.04	0.2	0.04
GNI	315	68.6	39	19.5	–	8.5	–	0.04	0.04	0
ARU	316	50.0	36	19.6	15.7	7.7	7.5	0.2	0.2	0.2
EIL	318	81.5	39	21.4	–	10.9	–	0.04	0.2	0
KIV	318	65.9	27	16.9	–	7.7	–	0.04	0.04	0
KSDI	319	78.0	45	17.8	–	8.9	–	0.04	0.04	0
TIXI	322	18.2	36	14.7	17.5	9.6	8.9	1	1	0.2
TIRR	328	69.6	36	15.3	15.3	10.4	8.5	0.04	1	1
KWP	334	66.1	39	15.9	14.5	10.8	10.7	1	0.2	0.2
PSZ	336	68.3	39	15.8	16.7	11.7	10.5	1	1	1
MORC	338	67.0	45	16.1	15.1	11.9	10.7	1	0.2	0.2
KEV	341	46.6	36	16.2	8.7	11.2	7.0	0.2	0.2	0.04
GRFO	342	68.1	33	10.6	18.5	8.7	9.6	0.04	0.04	0.04
KONO	346	58.6	36	11.3	13.5	9.5	10.0	0.2	0.2	0.2
KBS	352	39.8	48	15.4	–	12.4	–	0	0.04	0

Note: Subscripts 1 and 2 refer to the respective frequency bands; $RT = (e^{(2)})^{1/2}$; $w(1)$, $w(2)$ are weights for the two bands.
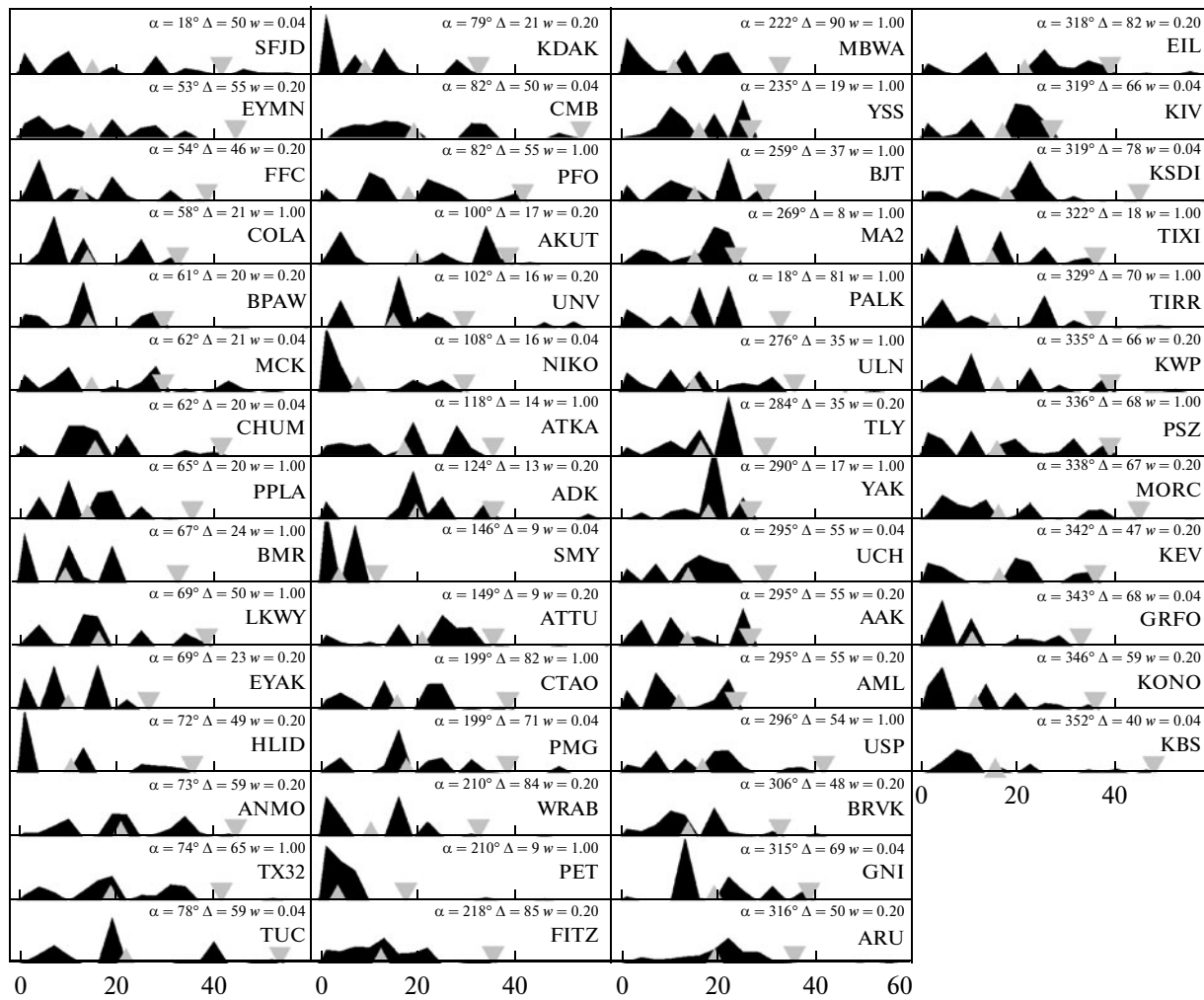
Fig. 5. Reconstructed source HFPSs for *P* waves in the band 0.7–1.7 Hz which were radiated toward the stations we used. Triangles mark temporal centroids, inverted triangles are estimates of T_f. At each record we give azimuth α, distance Δ°, and weight assigned *w*.

local network, we determine the centroid for the high frequency radiator (i.e., the middle of the linear segment that models the radiator). The centroid of this high frequency radiator is sufficiently close to the centroid of the seismic moment (i.e., the low frequency radiator) as found in the Harvard CMT solution.

Rupture kinematics and geometry. We assume, as is usually done, that the point of rupture initiation is identical with the hypocenter as located from data of teleseismic stations (60.95° N, 167.09° E). Considering that the vectors $\{F_x, F_y\}$, $\{M1_x, M1_y\}$ and $\{M_{xt}, M_{yt}\}$ have consistent directions, the rupture process tended to develop south-

Table 2. Estimates for the components of spatio-temporal vectors **F** and **M1**, their uncertainties and derivative parameters

Vector	N	Z_t, s	Z_x, km	Z_y, km	Z_L, km	Z_{az}, deg	Z_v, km/s
F	55	35.0	−61.5	−61.8	87.3	225	2.50
σ(F)		1.55	33.6	22.0	28.4	19	0.82
$M1_1$	57	14.9	−19.3	−3.1	19.5	189	1.30
σ($M1_1$)		0.69	14.9	9.65	12.5	37	0.85
$M1_2$	43	14.6	−19.3	−18.2	26.6	223	1.81
σ($M1_2$)		0.70	15.5	10.4	13	28	0.91

Note: The columns Z_t, Z_x, and Z_y contain the temporal and two spatial components of **F** and **M1**, the columns Z_L, Z_{az}, and Z_y contain derivative quantities, which are length L, azimuth az of the vectors, and the associated velocity (rupture velocity v in the case of L).
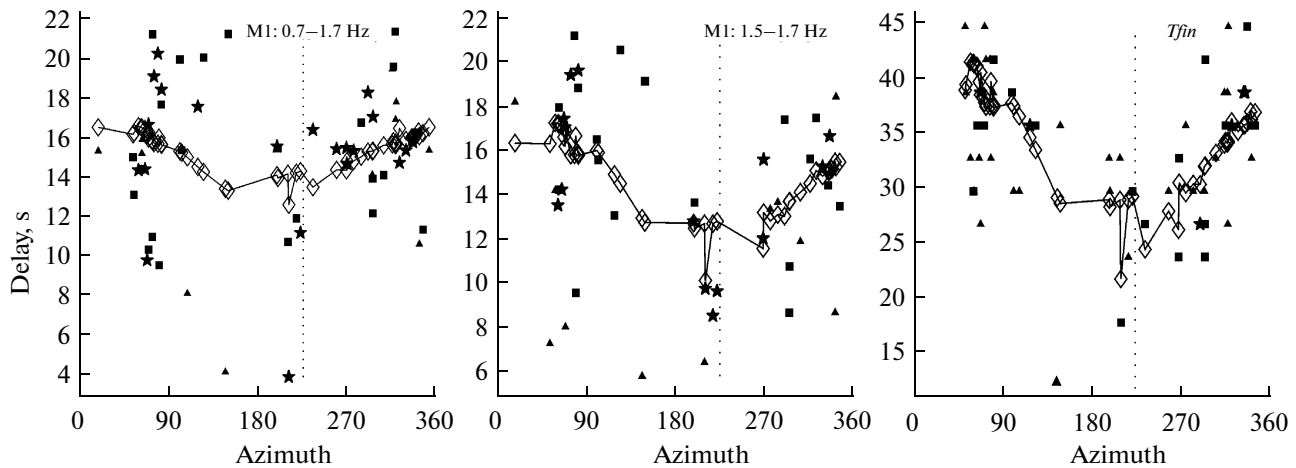
Fig. 6. Values of $e^{(1)}$ (for the two frequency bands) and T_f plotted against station azimuth. Diamonds connected by straight segments represent the theoretical relation found by LS. Symbols denote estimates based on observations; the weight of an estimate is increasing with increasing number of vertices the symbol involves. Vertical dashed line marks the fixed strike of the rupture (225°). The azimuthal asymmetry of the rupture clearly emerges from these plots, although upon the background of a large scatter.

westwards, but the rupture asymmetry was not strongly pronounced. The rupture propagated from the point of rupture initiation (in the framework of the linear segment model) to both sides along a 128-km linear feature striking southwest−northeast. Since the vectors of the first moments are relatively shorter and may be situated within the fault plane when this is sufficiently wide, we have adopted the estimate of rupture azimuth based on the vector **F** only. In that case the longer arm (87 km) strikes 225SW and the shorter arm (41 km) strikes 45NE. The rupture velocity was 2.5 km/s. This value should be compared with crustal shear velocity, about 3.5 km/s; the ratio of the two gives an ordinary value of the Mach number, 0.71. The position of the linear segment in the modeled source is in satisfactory agreement with the position and length of the aftershock zone, but the actual length of that zone (about 140 km) is somewhat greater than our estimate. The discrepancy is appreciable for the northeastern end of the aftershock zone.

We wish to note that the above model assumes the rupture velocities to be identical in both senses. Now as a matter of fact, we have only estimated the southwestward velocity. The northeastward velocity involves (along with the length of the northeastern rupture arm) some extra uncertainty. Analysis shows, however, that this extra uncertainty is actually restricted if the luminosity is assumed to be more or less uniformly distributed on both arms.

The radiation structure over time. Judging from the value of the temporal moment N_t, the temporal centroid is 15 s later than the rupture beginning on the time axis, or in other words, the average (over the entire rupture) radiation is delayed by 15 s relative to the "origin time." The total duration of the rupture process is $F_t = 35$ s. The value $2N_t = 29.5$ s gives another, cruder duration estimate in approximate agreement with $F_t = 35$ s. Lastly, the estimate based on M_{tt}, which equals $T^{(2)} = 28.5$ s, is also in approximate agreement with the two first.

Multiplying $T^{(2)}$ by $v_r = 2.5$ km/s gives an estimate of the characteristic length: $L^{(2)} = 71.2$ km. This should be compared with the mean of the lengths of the two rupture arms, equal to $128/2 = 64$ km. The agreement is quite satisfactory again.

Table 3. Estimates for the components of the spatio-temporal vector **M2**, their uncertainties and derivative parameters

Vector	N	Z_{tt}, s²	Z_{tx}, km s	Z_{ty}, km s	Z_{tL}, km s	Z_{az}, deg
$M2_1$	57	73.6	−145.5	−66.0	160.0	204
$\sigma(M2_1)$		≈10	≈64	≈38	≈77	≈45
$M2_2$	43	61.8	−105.1	−85.8	135.7	235
$\sigma(M2_2)$		≈15	≈100	≈63	≈120	≈50

Note: The columns Z_{tt}, Z_{tx}, and Z_{ty} contain the respective temporal component and two mixed spatio-temporal components of **M2**, the columns Z_{tL} and Z_{az} contain derivative quantities − length tl and azimuth az of the vector $\{M2_{tx}, M2_{ty}\}$. The following values have been fixed for the components M_{xx}, M_{xy}, and M_{yy}: 844.6, 646.4, and 579.2 km². The uncertainty estimates are rather crude.
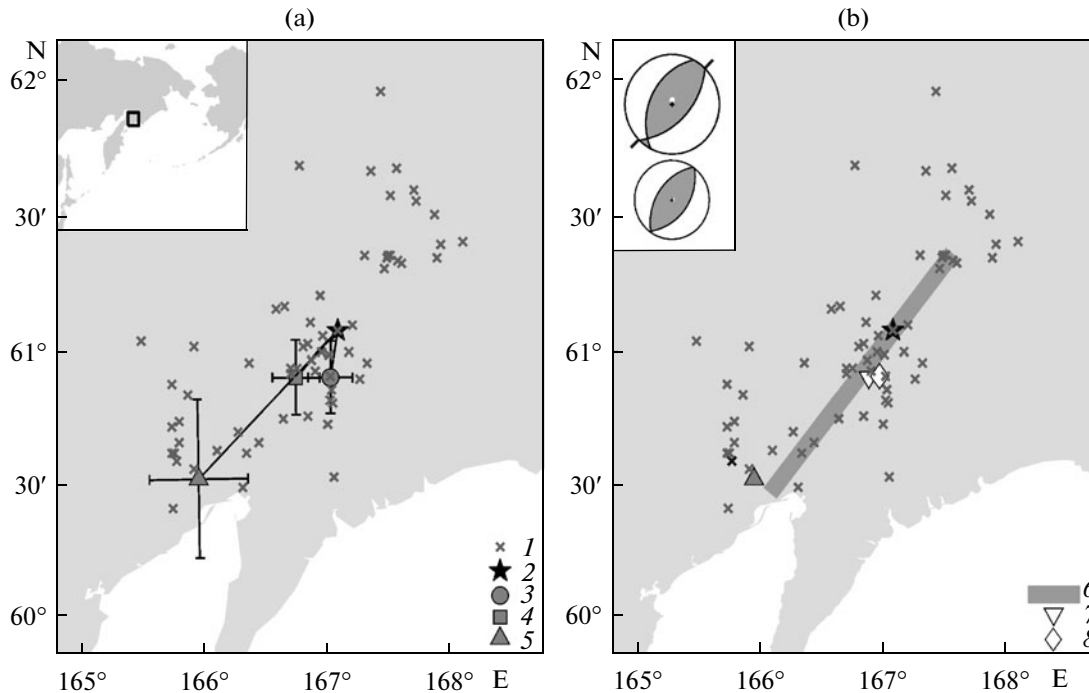
Fig. 7. Maps representing results of calculation. The maps show aftershock epicenters for April 20−23 as reported by the KB GS RAS (*1*); the symbol representing the epicenter of the aftershock used to correct the HFPS is enhanced by black; also shown is the mainshock epicenter (*2*) based on teleseismic data (NEIC USA). (a) estimated position of the radiator's centroid (*3* for the frequency band 0.7−1.7 Hz, *4* for 1.5−2.5 Hz), and the estimated position of rupture termination point (*5*). All estimates are accompanied by uncertainty ranges (±1σ) for the NS and EW directions. Inset shows the position of the area of study. (b) rupture reconstruction derived in this study in the form of a straight segment (*6*). Also shown are the mean centroid based on the two frequency bands (*7*) and the radiator's low frequency centroid as found in the Harvard CMT catalog (*8*). The inset shows, from top to bottom, the nodal planes for the main shock and the aftershock as reported in the Harvard CMT catalog (the lower hemisphere). We mark the strike direction (44°−224°) for the preferred nodal plane as appears from field geological data kindly provided by T.K. Pinegina.

CONCLUSIONS

This study provides a sufficiently complete description of the overall spatio−temporal structure of the high frequency radiator in the source zone of the earthquake studied. It may be presumed therefore that, to some approximation, the rupture geometry and kinematics have been reconstructed.

All numerical estimates of the source parameters derived here are assigned sufficiently definite uncertainty estimates. This fact, so ordinary on the face of it, is not actually ordinary: the level of inversion typical of the field of earthquake rupture reconstruction does not yield any well-defined uncertainties of the solutions. An analysis of the errors shows that some source parameters, such as map-view orientation (strike), rupture duration, and the degree of asymmetry are comparatively accurately estimated, while the estimates for rupture length and rupture velocity involve considerable uncertainties.

The reconstructed geometry of the high frequency rupture is in satisfactory agreement with other information relating to the rupture zone of this earthquake. The position and orientation of the rupture line are in agreement with the seismic moment centroid (CMT) and with the orientation of the preferred nodal plane of the respec-

tive double couple. The rupture position is in overall agreement with the geometry of the aftershock hypocenter cloud, but the northeastern termination of the cloud extends somewhat farther than required by the estimate we derived for the northeastern rupture termination.

REFERENCES

1. Gusev, A.A. and Pavlov, V.M., A Set of Integral Characteristics for an Earthquake Source Found from Body Wave Displacements Recorded in the Far Zone, *Dokl. AN SSSR*, 1978, vol. 39, no. 2, pp. 289−292.

2. Gusev, A.A. and Pavlov, V.M., The Method of Moments in the Problem of Reconstructing the Motion at the Earthquake Source from Its Radiation, *Vulkanol. Seismol.*, 1982, no. 5, pp. 61−82.

3. Gusev, A.A. and Pavlov, V.M., A Preliminary Determination of the Parameters for the High Frequency Radiator of the December 5, 1997 Kronotskii Earthquake (M_W = 7.9, Kamchatka), in *Kronotskoe zemletryasenie na Kamchatke 5 dekabrya 1997 g* (The Kronotskii

Earthquake of December 5, 1997 in Kamchatka), Petropavlovsk–Kamchatskii: KGARF, 1998, pp. 68–79.

4. Pavlov, V.M. and Gusev, A.A., On the Possibility of Reconstructing the Movement in the Rupture Zone of a Deep Earthquake from the Far-Zone Body Wave Field, *Dokl. AN SSSR,* 1980, vol. 255, pp. 834–828.

5. Gusev, A.A. and Pavlov, V.M., Determination of Space–Time Structure of a Deep Earthquake Source by Means of Power Moments, *Tectonophysics*, 1988, vol. 152, pp. 319–334.

6. Gusev, A.A. and Pavlov, V.M., Deconvolution of Squared Velocity Waveform as Applied to Study of Non-Coherent Short-Period Radiator in Earthquake Source, *Pure Appl. Geophys.,* 1991, vol. 136, pp. 235–244.

7. Gusev, A.A. and Pavlov, V.M., Preliminary Determination of Parameters of the High-Frequency Source for the Dec 05, 1997 $M_W = 7.9$ Kronotsky Earthquake, in *Papers XXVI Gen. Assembly Eur. Seismol. Commission*, Tel-Aviv, Israel, 1998, pp. 73–77.

8. Gusev, A.A., Guseva, E.M., and Panza, G.F., Size and Duration of the High-Frequency Radiator in the Source of the 2004 December 26 Sumatra Earthquake, *Geophys. J. Int.*, 2007, vol. 170, pp. 1119–1128.

9. Kakehi, Y. and Irikura, K., Estimation of High Frequency Wave Radiation Areas on the Fault Plane by the Envelope Inversion of Acceleration Seismograms, *Geophys. J. Int.*, 1996, vol. 125, pp. 892–900.

10. Nishimura, T., Nakahara, H., Sato, H., and Ohtake, M., Source Process of the 1994 Far East off Sanriku Earthquake, Japan, as Inferred from a Broad-Band Seismogram, *Sci. Rep. Tohoku Univ.*, 1996, vol. 34, pp. 121–134.

11. Petukhin, A.G., Nakahara, H., and Gusev, A.A., Inversion of the High-Frequency Source Radiation of M6.8 Avachinsky Gulf, Kamchatka, Earthquake Using Empirical and Theoretical Envelope Green Functions, *Earth, Planets and Space*, 2004, vol. 56, pp. 921–925.

12. Zeng, Y., Aki, K., and Teng, T.-L., Mapping of the High Frequency Source Radiation for the 1989 Loma Prieta Earthquake, California, *J. Geophys. Res.*, 1993, vol. 98, pp. 11 981–11?993.